

# Dissipative phase transition of interacting non-reciprocal fermions

Rafael D. Soares,<sup>1,2</sup> Matteo Brunelli,<sup>2</sup> and Marco Schirò<sup>2</sup>

<sup>1</sup>Max Planck Institute for the Physics of Complex Systems, Nöthnitzer Straße 38, 01187 Dresden, Germany

<sup>2</sup>JEIP, UAR 3573 CNRS, Collège de France, PSL Research University,  
11 Place Marcelin Berthelot, 75321 Paris Cedex 05, France

(Dated: June 13, 2025)

We study an interacting fermionic chain in the presence of non-reciprocal gain and loss processes obtained via reservoir engineering. The interplay between unitary evolution and the two dissipative processes leads to distinct non-reciprocal signatures in the transient dynamics and the steady state. These include a transition from exponential to power-law relaxation towards a finite-density steady-state, a nonzero particle current from breaking inversion symmetry, and dynamics under open boundary conditions showing directionality and charge accumulation. Weak interactions preserve the main signatures of non-reciprocity, enriching the interacting many-body non-reciprocal phase with volume law entanglement of quantum trajectories. Upon increasing the interaction above a critical value, we find a dissipative phase transition where reciprocity is dynamically restored.

*Introduction* – For classical and quantum systems in thermal equilibrium, the interactions between degrees of freedom are fundamentally symmetric or reciprocal. Far from equilibrium, however, asymmetric or non-reciprocal interactions are ubiquitous. Examples range from optics [1, 2], to active [3–6] or living matter [7], ecology [8, 9], robotic systems [10] and statistical physics [11–14]. Non-reciprocal systems display unusual properties, including unique critical behavior at phase transitions [15].

First investigated for classical systems, interest in non-reciprocity has branched out to the quantum world. Non-reciprocal phenomena can naturally arise in non-Hermitian quantum mechanics [16], the Hatano-Nelson model providing a well-known example of a system with non-reciprocal hopping [17, 18], leading to rich physics such as enhanced sensitivity to boundary conditions, the so-called non-Hermitian skin effect [19–21], non-Hermitian topology [22, 23] and entanglement phase transitions [24]. However, this approach neglects the contribution from quantum jumps. A fully consistent quantum-mechanical treatment of non-reciprocity is possible within the framework of cascaded master equations [25, 26] and reservoir engineering [27, 28].

The first steps towards applying these ideas to open quantum many-body systems [29] have recently been taken [30–41]. Outstanding questions are whether quantum many-body systems can exhibit robust non-reciprocal steady states featuring rich entanglement structures, akin to those found in their non-Hermitian counterparts, and whether quantum non-reciprocal phase transitions connecting such states can exist. In addition, one could ask whether these phase transitions can be classified within the framework of dissipative phase transitions or whether they instead represent a new universality class [42].

In this Letter, we consider an interacting fermionic chain with non-reciprocity, obtained via reservoir engineering of both gain and loss processes, as sketched in

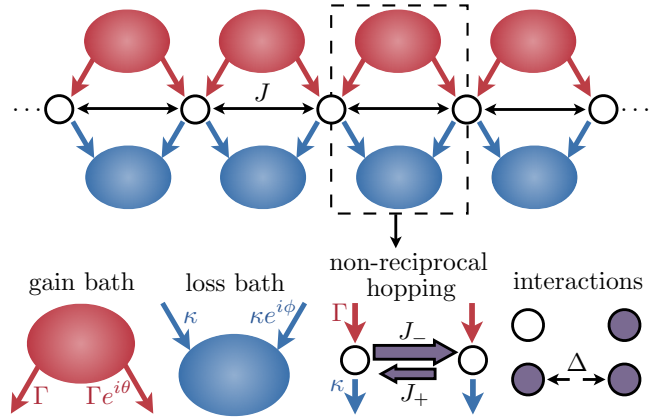


Figure 1. Sketch of the setup: one-dimensional fermionic chain with nearest-neighbor hoppings,  $J$ , and density-density interaction,  $\Delta$ . The gain (loss) bath injects (absorbs) particles to (from) neighboring sites, with relative phase  $\theta$  ( $\phi$ ). Together with the hopping term, they realize non-reciprocal gain and loss processes.

Fig. 1. Specifically, we consider neighboring sites of the chain to be dissipatively coupled via an active and a passive reservoir, each of which breaks the time-reversal symmetry and is described by an asymmetric coupling matrix. We refer to these two engineered processes as non-reciprocal gain and loss, respectively. We show that the competition between non-reciprocal gain and loss and the coherent evolution gives rise to a genuine criticality, i.e., a vanishing dissipative gap leading to universal power-law decay of physical quantities towards a finite-density steady state. This stands in stark contrast to the case of purely local gain, recently studied in Ref. [36], whose long-time behavior is always exponential. Beyond non-reciprocal hopping, non-reciprocal gain and loss give rise to unique signatures, including a finite steady-state current arising from a non-thermal occupation, breaking inversion symmetry, and charge accumulations at the edges of the system with open boundary conditions. Re-

markably, we show that these features are robust to interactions. Namely, we demonstrate the existence of a non-reciprocal interacting many-body phase displaying power-law dynamics and charge accumulation, yet it sustains volume-law entanglement in the quantum trajectory unraveling of the steady-state. Upon increasing interactions above a critical value, the dynamics becomes exponential, indicating the opening of a many-body dissipative gap via a phase transition where reciprocity is dynamically restored, which we attribute to an instability towards charge density wave. Our work highlights the role of non-reciprocal gain and loss in giving rise to exotic dynamical and steady-state properties.

*Model and Setup* – We consider an interacting fermionic chain of size  $L$  described by the Hamiltonian

$$\mathcal{H} = -\frac{J}{2} \sum_{j=1}^{L-1} [c_j^\dagger c_{j+1} + c_{j+1}^\dagger c_j] + \Delta \sum_{j=1}^{L-1} n_j n_{j+1}, \quad (1)$$

where  $c_j^\dagger$  ( $c_j$ ) is the fermionic creation(annihilation) operator that creates(annihilates) a particle at site  $j$ ,  $n_j = c_j^\dagger c_j$ ,  $J$  is the hopping strength and  $\Delta$  is the next-neighbor density-density interaction, see Fig. 1. We are interested in the dissipative dynamics generated by the Lindblad master equation for the system density matrix  $\rho$  [29]

$$\partial_t \rho = -i[\mathcal{H}, \rho] + \sum_{j,\mu} L_{j,\mu} \rho L_{j,\mu}^\dagger - \frac{1}{2} \left\{ L_{j,\mu}^\dagger L_{j,\mu}, \rho \right\}, \quad (2)$$

where  $L_{j,\mu}$  are a set of jump operators describing non-local gain and losses ( $\mu = g, \ell$  respectively) with strength  $\Gamma, \kappa$ . Specifically, we take these of the form [32]

$$L_{j,\ell} = \sqrt{\kappa} (c_j + e^{i\phi} c_{j+1}), \quad L_{j,g} = \sqrt{\Gamma} (c_j^\dagger + e^{i\theta} c_{j+1}^\dagger). \quad (3)$$

These jump operators can be realized within the framework of reservoir engineering [27, 34, 43–46]. Similar jump operators in the non-interacting setting have been discussed before [32]. For  $\theta, \phi \neq 0$  the jump operators in Eq. (3) give rise to asymmetric gain and loss matrices i.e. to non-reciprocal dissipative couplings. In the absence of coherent hopping ( $J = 0$ ), one of the two phases can be removed from the Lindblad master equation by a local gauge transformation [47]. On the other hand, for  $J \neq 0$ , the two phases give rise to a rich landscape of non-reciprocal behavior in dynamic and static properties, as we are going to show below.

*Non-Interacting Limit* – We start by discussing the non-interacting limit  $\Delta = 0$ , which provides useful insight. The dynamics of the correlation matrix  $C_{ij} = \langle c_i^\dagger c_j \rangle$  takes the form

$$i\partial_t C_{ij} = \sum_l (H)_{jl} C_{il} - (H^\dagger)_{li} C_{lj} + iG_{ij}, \quad (4)$$

where  $(H)_{jl} = -2i(\kappa + \Gamma)\delta_{jl} - \frac{1}{2}J_+\delta_{j,l+1} - \frac{1}{2}J_-\delta_{j,l-1}$  encodes an effective non-Hermitian Hamiltonian associated to the unconditional evolution, which is different

from the no-click limit [34], and noise matrix  $G_{jl} = \Gamma(e^{-i\theta}\delta_{j,l+1} + e^{i\theta}\delta_{j,l-1} + 2\delta_{j,l})$ . In our case  $H$  takes the form of the Hatano-Nelson model [17] with hopping amplitudes

$$J_\pm = J + i(\Gamma \cos \theta + \kappa \cos \phi) \pm (\Gamma \sin \theta - \kappa \sin \phi). \quad (5)$$

Unequal amplitudes  $J_+ \neq J_-$  signify non-reciprocal hopping.

For periodic boundary conditions (PBC), the problem can be solved exactly in Fourier space, leading to a momentum-dependent pump rate  $\Gamma_k = 2\Gamma(1 + \cos(k - \theta))$  and losses  $\kappa_k = 2\kappa(1 + \cos(k + \phi))$ . Solving for the dynamics of the occupation numbers [47]  $\langle n_k \rangle = \langle c_k^\dagger c_k \rangle$ , we obtain

$$\langle n_k(t) \rangle = \langle n_k \rangle_{\text{ss}} + e^{-\lambda_k t} (\langle n_k(0) \rangle - \langle n_k \rangle_{\text{ss}}), \quad (6)$$

where  $\lambda_k = \Gamma_k + \kappa_k$  represents the spectrum of decay rates and can be written using Eq. (5) as

$$\lambda_k = 2(\Gamma + \kappa) + \text{Im}(J_+ + J_-) \cos k + (J_+ - J_-) \sin k, \quad (7)$$

while  $\langle n_k \rangle_{\text{ss}} = 1/(1 + \kappa_k/\Gamma_k)$  is the steady-state distribution which reads

$$\langle n_k \rangle_{\text{ss}} = \frac{\Gamma(1 + \cos \theta \cos k + \sin \theta \sin k)}{2(\Gamma + \kappa) + \text{Im}(J_+ + J_-) \cos k + (J_+ - J_-) \sin k}. \quad (8)$$

We make several observations. First, we note that the phases of momentum-dependent gain and losses  $\theta, \phi$  enter differently in the spectrum  $\lambda_k$  and in the steady-state occupation  $\langle n_k \rangle_{\text{ss}}$ . As a result, the two dissipative processes give rise to distinct non-reciprocal behavior in the dynamics or in the stationary state. We start by discussing the spectrum and the dynamics. From Eq. (7), we see that the slowest decaying mode is at  $k_* = \arctan[(\Gamma \sin \theta - \kappa \sin \phi) / (\Gamma \cos \theta + \kappa \cos \phi)]$  and around this value the spectrum reads  $\lambda_k = \delta + \alpha(k - k_*)^2$ , with the dissipative gap

$$\delta = 2(\Gamma + \kappa) - 2\sqrt{\Gamma^2 + \kappa^2 + 2\Gamma\kappa \cos(\theta + \phi)}. \quad (9)$$

In the  $\phi, \theta$  plane the gap is finite everywhere, except along the line  $\theta = -\phi$  where it closes, as we show in Fig. 2(a). This implies that an excitation with wavevector  $k_*$  is not affected by dissipation and evolves due to the unitary part of evolution alone [47]. The existence of this gapless mode has direct consequences on the system's dynamics, making observables, such as the particle density, approach the steady state following a universal power-law decay [47]  $\langle n(t) \rangle = \int dk \langle n_k \rangle \sim \langle n \rangle_{\text{ss}} - \delta n / \sqrt{t}$ . Moving away from this line the dissipative gap opens and the dynamics becomes exponential; see Fig. 2(b). This corresponds to a dissipative transition where the time scale to reach the steady-state diverges. We emphasize that this critical dynamics is the result of a balance between momentum dependent gain

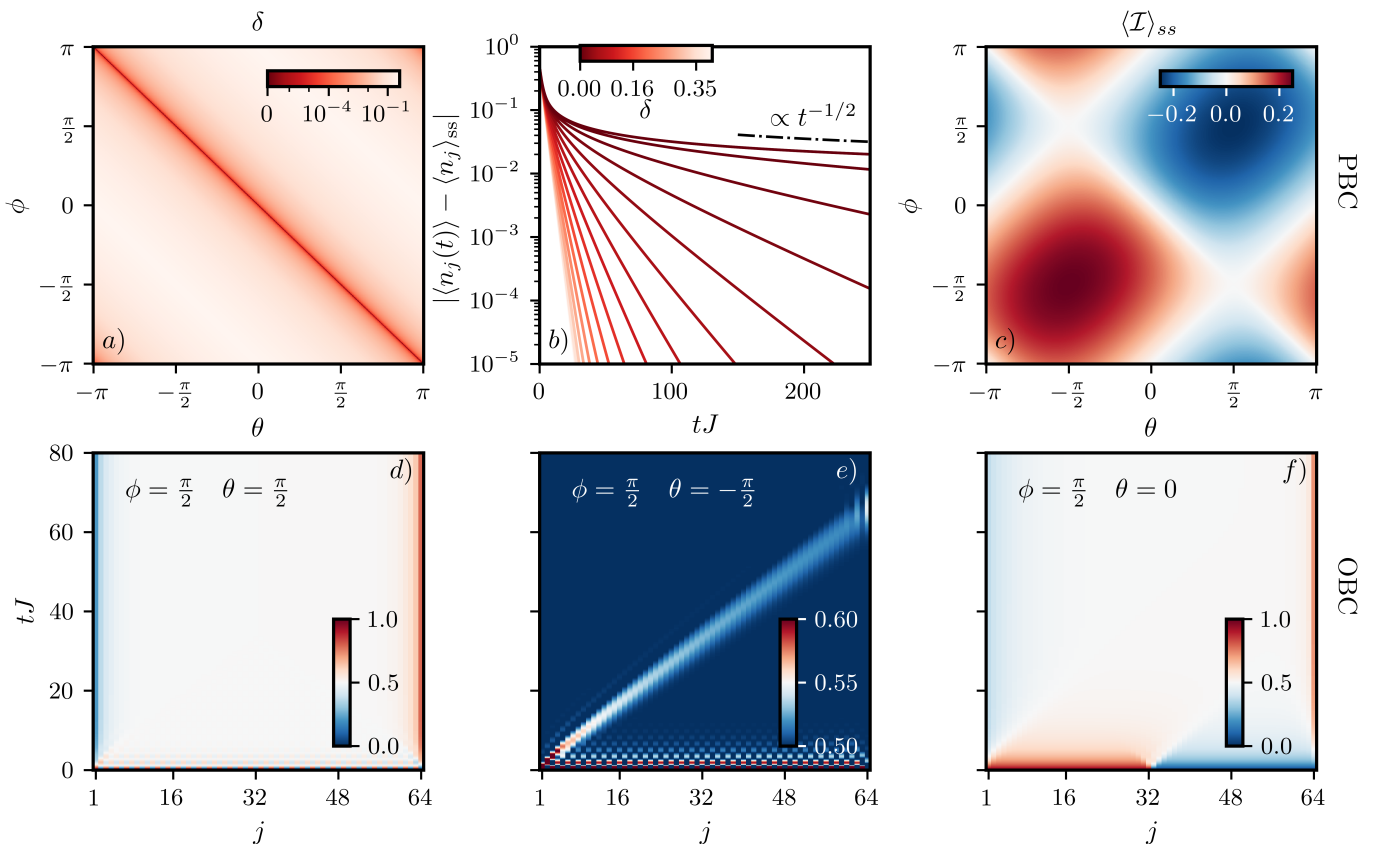


Figure 2. *a*) - Dissipative gap  $\delta$  as a function of the angles  $\theta$  and  $\phi$ . A symlog scale is used in the colormap to highlight that this value only vanishes for  $\theta = -\phi$ . *b*) - Time evolution of the particle density (rescaled by the steady-state value) for different values  $\delta$ . *c*) - Steady-state particle current in PBC as a function of the angles. In the bottom row *d*), *e*) and *f*), we depict the particle density dynamics with OBC for different values of the angles. In both panel *d*) and *e*), the initial state corresponds to a CDW, while in panel *f*) it corresponds to a domain-wall. In panel *e*), we have truncated the colormap to highlight the directionality in the propagation. Other parameters:  $\Gamma = \kappa = 0.1J$ .

and loss, which is absent for local gain where the system is always gapped [36]. The dynamics along the line  $\phi = -\theta$  shows non-reciprocal features, since the spectrum is asymmetric in momentum space  $\lambda_k - \lambda_{-k} = 2(J_+ - J_-) \sin k$ , leading to a non-reciprocal transient occupation  $\langle n_{-k}(t) \rangle \neq \langle n_k(t) \rangle$  and so to a non-zero transient current  $\langle \mathcal{I} \rangle = -J \int dk \sin k \langle n_k \rangle \sim \mathcal{I}_0 \sin \phi / \sqrt{t}$  that slowly vanishes at long times with a magnitude controlled by the phase of the gain and loss baths [47].

We now discuss the steady-state distribution Eq.(8), which features two distinct sources of non-reciprocity, namely, from the spectrum (denominator) and from the non-reciprocal gain (numerator). This leads to a non-trivial distribution across the  $\theta, \phi$  plane. For example, along the line  $\theta = \phi$  and for  $\Gamma = \kappa$ , where the hopping is reciprocal ( $J_+ = J_-$ ), the steady-state distribution in Eq. (8) is highly non-thermal [47]. Furthermore, the presence of non-reciprocal gain breaks inversion symmetry, as reflected from  $\langle n_{-k} \rangle_{ss} \neq \langle n_k \rangle_{ss}$ . This asymmetry results in a finite steady-state current, which reaches its maximum at  $\theta = \phi = \pi/2$  [47]. On the other

hand, along the line  $\phi = -\theta$ , the two dissipative processes interfere destructively and the distribution simplifies to  $\langle n_k \rangle_{ss} = \Gamma / (\Gamma + \kappa)$ , i.e. it becomes flat in momentum space and as a consequence the steady-state current vanishes, just as in the case of local bulk gain and losses. When plotted in the plane  $\phi, \theta$ , the steady-state current shows a diamond structure reminiscent of Coulomb blockade physics [48], with lines of zero and maximal currents that arise due to interference between the dissipative processes; see Fig. 2(c). The steady-state correlation matrix decays exponentially across the phase diagram with a length that grows approaching the line  $\phi = -\theta$  [47]. However, when the dissipative gap closes also the momentum dependent gain vanishes, preventing the correlation length to diverge [49, 50]. The dissipative transition that occurs when  $\theta, \phi$  are tuned along the critical line  $\theta = -\phi$  is directly visible in the retarded Green function of the system, encoding the spectrum of finite frequency excitations above the steady-state while the distribution function displays effective thermal behavior [47].

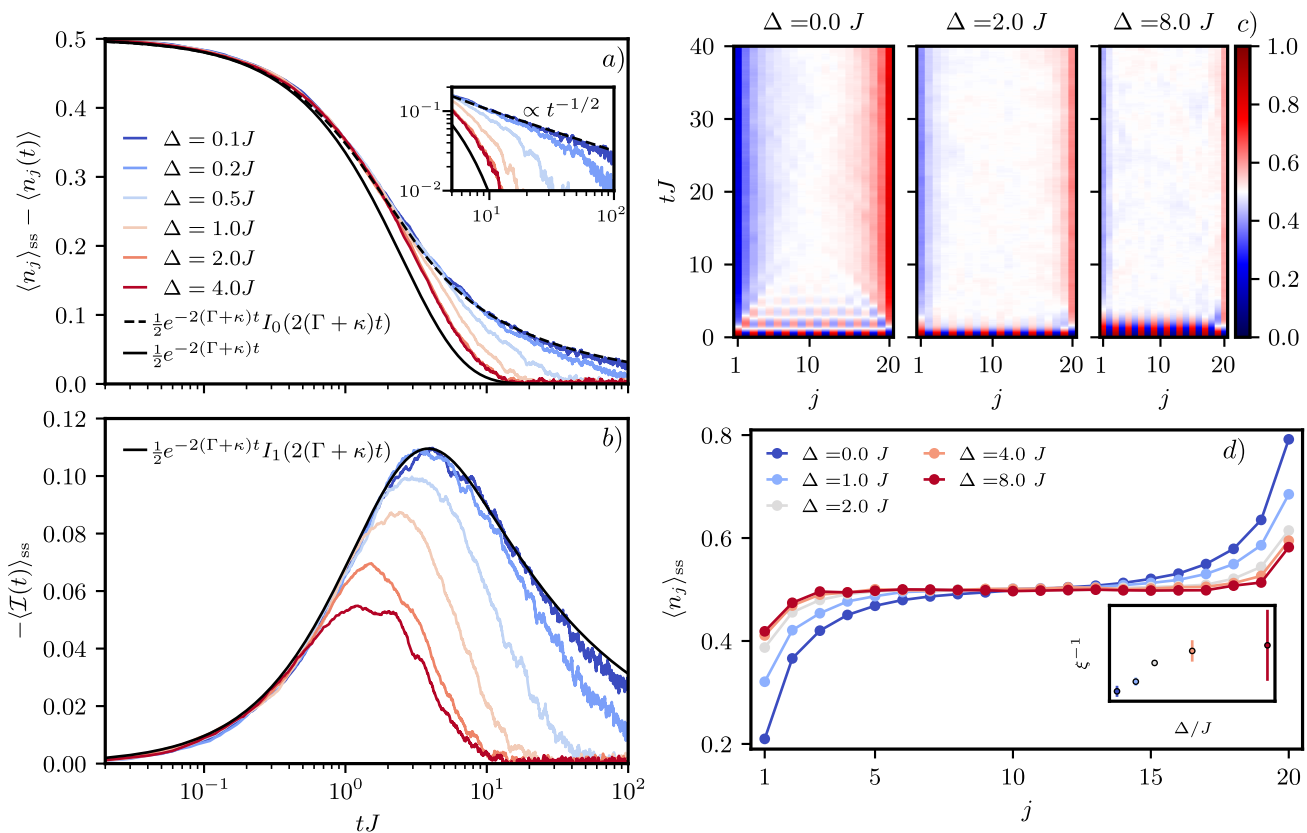


Figure 3. Time evolution of *a*) the particle density (rescaled by the steady-state value) and *b*) the particle current for different values of the interaction strength  $\Delta$  with PBC; the system has  $L = 16$  and is initialized in the empty state. *c*) Time evolution of the particle density and *d*) its value in the steady state for different values of  $\Delta$  and with OBC. The system has  $L = 20$  and is initially in a charge density wave configuration. In panel *a*) and *b*)  $\phi = -\theta = \pi/2$ , while in panel *c*) and *d*)  $\phi = \theta = \pi/2$ . Other parameters:  $\Gamma = \kappa = 0.1J$ .

We now consider the dynamics with open boundary conditions (OBC) [51]. In Fig. 2(d-f) (bottom panels), we plot the dynamics of the particle density for different values of  $\theta, \phi$  and different initial states, at  $\Gamma = \kappa$ . For  $\theta = \phi = \pi/2$ , the initial charge-density wave (CDW) is quickly melted in the bulk after few short-time revivals, in agreement with the previous discussion of exponential dynamics. However, at the edges the dynamics is nontrivial: charge is reshuffled across the system by the non-reciprocal gain and loss, and we observe the build up of a steady state featuring charge accumulation at the edges, see Fig. 2(d). Upon tuning the angle  $\theta$  we see that the charge imbalance decreases and eventually disappears for  $\theta = -\pi/2$ , a value at which, however, the dynamics displays clear directionality; see Fig. 2(e).

We can understand these results by looking at the non-reciprocal hopping rates  $J_{\pm}$  in Eq. (5). For  $\Gamma = \kappa$  the maximum value of  $J_{+} - J_{-}$  is obtained precisely for  $\phi = \pi/2 = -\theta$ , while for  $\theta = \phi = \pi/2$  the hopping is perfectly reciprocal and so the dynamics. Overall, this behavior is reminiscent of the dynamics of the Hatano-Nelson model, yet it appears at the level of a fully Lindbladian evolution

Eq. (4), which includes dissipation and noise and does not require post-selection [52]. Finally, for intermediate values of the angles and an initial state which is a domain wall, the dynamics displays directional features in the bulk as well as charge accumulation; see Fig. 2(f).

*Role of Interactions* – We now move to the interacting case and solve the problem by unraveling Eq. (2) into quantum jump trajectories [29, 53–55]. In order to perform the non-Hermitian evolution between subsequent quantum jumps, we make use of the recently developed Faber polynomial method [47, 56]. We consider a finite chain and fix the gain and loss to be equal,  $\Gamma = \kappa = 0.1J$ . We first discuss the PBC case and fix  $\theta = -\phi = -\pi/2$  to see whether the power-law behavior observed in the dynamics of non-interacting fermions survives for finite interactions. In Fig. 3(a) we plot the dynamics of particle density for different values of  $\Delta$ . At short times interaction effects are negligible; however, at longer time scales the decay toward the steady state strongly depends on  $\Delta$ . Remarkably, we see that for weak  $\Delta$  the dynamics is compatible with a power-law (the dashed line corresponds to the power-law behavior in the non-interacting

case), possibly with an interaction-dependent exponent. For higher values of  $\Delta \sim J$ , on the other hand, the decay of the particle density is faster, crossing over to an exponential decay set by the total dissipation rate  $\Gamma + \kappa$ . This points towards a genuine dissipative phase transition in the system, due to interactions and non-reciprocity. Similar behavior is observed for the current in Fig. 3(b) which for the chosen values of  $\theta, \phi$  decays to zero at long times. First, we observe a peak in the time-dependent current at intermediate times, which is renormalized by interactions in magnitude and pushed to shorter time scales. At long times, we see that for  $\Delta < J$  the decay is compatible with a power-law, while at larger  $\Delta$  the current quickly vanishes at long times.

We now discuss the role of interactions in the OBC case. We consider the dynamics of the average particle density  $\langle n_j(t) \rangle$  starting from a CDW state,  $|\Psi(0)\rangle = |1010\dots\rangle$  and for different values of interaction  $\Delta$ . We fix the value of phases to  $\theta = \phi = \pi/2$ , corresponding to boundary charge accumulation in the non-interacting case (see Fig. 2(d)). Here, we focus on the effect of interactions on the charge dynamics. As we show in Fig. 3(a) increasing  $\Delta$  has two major effects: (i) the tendency toward charge accumulation at the boundaries is reduced, although not suppressed completely even for  $\Delta = 8J$ , and (ii) the initial CDW state remains frozen for a longer time. These two effects are indeed connected and result from an interaction-induced renormalization of non-reciprocal gain and loss. To understand this point, we can proceed perturbatively and derive an effective model in the regime  $\Delta \gg J, \Gamma, \kappa$ . By going into a rotating frame we obtain new jump operators that read (analogous expression for gain) [47]

$$\tilde{L}_{j,\ell} = \sqrt{\kappa}(e^{i\Delta(n_{j-1}+n_{j+1})t}c_j + e^{i\phi}e^{i\Delta(n_j+n_{j+2})t}c_{j+1}) \quad (10)$$

In this rotating frame the Lindbladian is time-periodic with terms rapidly oscillating at frequency  $\omega \sim \Delta$  in the strongly interacting regimes, that can be averaged out as in the high-frequency expansion of Floquet systems [57–59]. From Eq. (10) we see that if neighboring sites are doubly occupied, the corresponding dissipative process is highly off-resonant in the regime  $\Delta \gg J$  and therefore effectively blocked. This simple argument explains why in the strongly interacting regime the initial CDW state, containing no doublons, remains long-lived and the non-reciprocal gain and loss become less efficient, reducing the charge accumulation at the edge.

We now characterize in more detail the structure of the steady-state density profile, which we plot in Fig. 3(d) for different values of  $\Delta$  and the same values of gain/loss  $\kappa = \Gamma = 0.1J$  and still for  $\phi = \theta = \pi/2$ . We see that the charge density in the bulk is pinned to half-filling, corresponding to a maximally mixed state due to equal gain and loss rates. The left(right) boundary displays charge depletion(accumulation), with a decay

towards the bulk that is compatible with an exponential law  $|\langle n_j \rangle_{\text{ss}} - \langle n_{L/2} \rangle_{\text{ss}}| = 1/2 + Ae^{-j/\xi}$  where  $\xi$  is the localization length and  $A$  a fitting constant. In the inset, we plot the inverse localization length  $\xi^{-1}$  that increases with the interaction  $\Delta$  and appears to saturate for  $\Delta/J \gg 1$ . Overall, these results suggest that interactions compete with the non-reciprocal gain and loss terms to reduce the tendency toward charge accumulation. Yet, our numerical results support the emergence of a robust non-reciprocal interacting many-body state at intermediate couplings. This conclusion is further supported by results along the  $\theta = -\phi$  line, showing that the directional dynamics seen in Fig. 2(e) is robust to moderate interactions (see End Matter for details). Quite interestingly, in this regime, although the charge is localized at the edges and the skin effect would lead to area-law entanglement of non-Hermitian free fermions [24], the unraveled steady-state for the interacting problem shows volume-law entanglement (see End Matter for details).

*Conclusions* – In this work we studied the dynamics of an interacting fermionic chain with non-reciprocal gain and loss processes, mediated by engineered active and passive baths that break time reversal symmetry. The combination of these two processes is key to obtain a genuine criticality, with a dissipative gap vanishing along the line  $\theta = -\phi$ , resulting in universal power-laws in the approach to the steady state in the periodic boundary condition case. Away from this line, the dynamics is exponential while the non-reciprocal steady state supports a non-zero current resulting from a steady-state distribution function breaking inversion symmetry. For open boundary conditions, the interplay between the two non-reciprocal processes manifest in charge accumulation and directional dynamics. Importantly, we have shown that these features are robust to interactions, which drive the system towards a genuine dissipative phase transition where the dynamics becomes again exponential. For OBC, the interactions renormalize the dissipative processes, reducing charge accumulation at the boundaries and promoting a charge density wave order in the bulk. Although the interacting non-reciprocal steady-state has a density profile reminiscent of a skin effect, its entanglement content is compatible with a volume law scaling. Our work showcases a rich pattern of transport, dynamics and entanglement properties arising from the combination of non-reciprocal dissipative couplings and coherent interactions.

*Acknowledgements* – We acknowledge A. Clerk, G. Lee and A. Pocklington for inspiring discussions. M.B and M.S. acknowledge funding from the European Research Council (ERC) under the European Union’s Horizon 2020 research and innovation program (Grant agreement No. 101002955 – CONQUER). We acknowledge Collège de France IPH cluster where the numerical calculations were carried out.

- [1] C. Caloz, A. Alù, S. Tretyakov, D. Sounas, K. Achouri, and Z.-L. Deck-Léger, *Phys. Rev. Appl.* **10**, 047001 (2018).
- [2] D. L. Sounas and A. Alù, *Nature Photonics* **11**, 774 (2017).
- [3] Z. You, A. Baskaran, and M. C. Marchetti, *Proceedings of the National Academy of Sciences* **117**, 19767 (2020), <https://www.pnas.org/doi/pdf/10.1073/pnas.2010318117>.
- [4] S. Saha, J. Agudo-Canalejo, and R. Golestanian, *Phys. Rev. X* **10**, 041009 (2020).
- [5] A. Poncet and D. Bartolo, *Phys. Rev. Lett.* **128**, 048002 (2022).
- [6] F. Brauns and M. C. Marchetti, *Phys. Rev. X* **14**, 021014 (2024).
- [7] T. H. Tan, A. Mietke, J. Li, Y. Chen, H. Higinbotham, P. J. Foster, S. Gokhale, J. Dunkel, and N. Fakhri, *Nature* **607**, 287 (2022).
- [8] V. Ros, F. Roy, G. Biroli, G. Bunin, and A. M. Turner, *Phys. Rev. Lett.* **130**, 257401 (2023).
- [9] E. Blumenthal, J. W. Rocks, and P. Mehta, *Phys. Rev. Lett.* **132**, 127401 (2024).
- [10] M. Brandenbourger, X. Locsin, E. Lerner, and C. Coulais, *Nature Communications* **10**, 4608 (2019).
- [11] G. G. Lorenzana, A. Altieri, G. Biroli, M. Fruchart, and V. Vitelli, *Non-reciprocal spin-glass transition and aging* (2024), [arXiv:2408.17360](https://arxiv.org/abs/2408.17360) [cond-mat.dis-nn].
- [12] R. Hanai, *Phys. Rev. X* **14**, 011029 (2024).
- [13] Y. Avni, M. Fruchart, D. Martin, D. Seara, and V. Vitelli, *Phys. Rev. Lett.* **134**, 117103 (2025).
- [14] J. T. Young, A. V. Gorshkov, and M. Maghrebi, *Nonequilibrium universality of the nonreciprocally coupled  $\mathbf{O}(\mathbf{n}_1) \times \mathbf{O}(\mathbf{n}_2)$  model* (2024), [arXiv:2411.12680](https://arxiv.org/abs/2411.12680) [cond-mat.stat-mech].
- [15] M. Fruchart, R. Hanai, P. B. Littlewood, and V. Vitelli, *Nature* **592**, 363 (2021).
- [16] Z. G. Yuto Ashida and M. Ueda, *Advances in Physics* **69**, 249 (2020), <https://doi.org/10.1080/00018732.2021.1876991>.
- [17] N. Hatano and D. R. Nelson, *Phys. Rev. Lett.* **77**, 570 (1996).
- [18] N. Hatano and D. R. Nelson, *Phys. Rev. B* **56**, 8651 (1997).
- [19] T. E. Lee, *Phys. Rev. Lett.* **116**, 133903 (2016).
- [20] S. Yao and Z. Wang, *Phys. Rev. Lett.* **121**, 086803 (2018).
- [21] N. Okuma and M. Sato, *Annual Review of Condensed Matter Physics* **14**, 83 (2023).
- [22] Z. Gong, Y. Ashida, K. Kawabata, K. Takasan, S. Higashikawa, and M. Ueda, *Phys. Rev. X* **8**, 031079 (2018).
- [23] K. Kawabata, K. Shiozaki, M. Ueda, and M. Sato, *Phys. Rev. X* **9**, 041015 (2019).
- [24] K. Kawabata, T. Numasawa, and S. Ryu, *Phys. Rev. X* **13**, 021007 (2023).
- [25] C. W. Gardiner, *Phys. Rev. Lett.* **70**, 2269 (1993).
- [26] H. J. Carmichael, *Phys. Rev. Lett.* **70**, 2273 (1993).
- [27] A. Metelmann and A. A. Clerk, *Phys. Rev. X* **5**, 021025 (2015).
- [28] A. A. Clerk, *SciPost Phys. Lect. Notes*, 44 (2022).
- [29] R. Fazio, J. Keeling, L. Mazza, and M. Schirò, *Many-body open quantum systems* (2025), [arXiv:2409.10300](https://arxiv.org/abs/2409.10300) [quant-ph].
- [30] M. Keck, D. Rossini, and R. Fazio, *Phys. Rev. A* **98**, 053812 (2018).
- [31] R. Hanai, A. Edelman, Y. Ohashi, and P. B. Littlewood, *Phys. Rev. Lett.* **122**, 185301 (2019).
- [32] F. Song, S. Yao, and Z. Wang, *Phys. Rev. Lett.* **123**, 170401 (2019).
- [33] F. Yang, Q.-D. Jiang, and E. J. Bergholtz, *Phys. Rev. Res.* **4**, 023160 (2022).
- [34] A. McDonald, R. Hanai, and A. A. Clerk, *Phys. Rev. B* **105**, 064302 (2022).
- [35] E. I. R. Chiacchio, A. Nunnenkamp, and M. Brunelli, *Phys. Rev. Lett.* **131**, 113602 (2023).
- [36] S. E. Begg and R. Hanai, *Phys. Rev. Lett.* **132**, 120401 (2024).
- [37] P. Brighi and A. Nunnenkamp, *Phys. Rev. A* **110**, L020201 (2024).
- [38] T. Nadolny, C. Bruder, and M. Brunelli, *Phys. Rev. X* **15**, 011010 (2025).
- [39] T. Nadolny, M. Brunelli, and C. Bruder, *Phys. Rev. Lett.* **134**, 193603 (2025).
- [40] C. P. Zelle, R. Daviet, A. Rosch, and S. Diehl, *Phys. Rev. X* **14**, 021052 (2024).
- [41] R. Belyansky, C. Weis, R. Hanai, P. B. Littlewood, and A. A. Clerk, *Phase transitions in nonreciprocal driven-dissipative condensates* (2025), [arXiv:2502.05267](https://arxiv.org/abs/2502.05267) [quant-ph].
- [42] L. M. Sieberer, M. Buchhold, J. Marino, and S. Diehl, *Universality in driven open quantum matter* (2023), [arXiv:2312.03073](https://arxiv.org/abs/2312.03073) [cond-mat.stat-mech].
- [43] D. Malz and A. Nunnenkamp, *Phys. Rev. B* **97**, 165308 (2018).
- [44] C. C. Wanjura, M. Brunelli, and A. Nunnenkamp, *Nat. Commun.* **11**, 3149 (2020).
- [45] D. Porras and S. Fernández-Lorenzo, *Phys. Rev. Lett.* **122**, 143901 (2019).
- [46] M. Brunelli, C. C. Wanjura, and A. Nunnenkamp, *SciPost Phys.* **15**, 173 (2023).
- [47] See supplemental material, where we provide additional results and detail the numerical and analytical methods used in this work. it includes refs. [29, 32, 42, 55, 56, 58–63].
- [48] Y. V. Nazarov and B. M. Yaroslav, *Quantum transport: introduction to nanoscience* (Cambridge Univ. Press, Cambridge, 2009).
- [49] Y. Zhang and T. Barthel, *Phys. Rev. Lett.* **129**, 120401 (2022).
- [50] T. Barthel and Y. Zhang, *Journal of Statistical Mechanics: Theory and Experiment* **2022**, 113101 (2022).
- [51] To ensure that all sites are subject to the same overall particle gain and losses, we add an extra loss/gain processes at the boundaries, described by jump operators  $L_{0,\ell} = \sqrt{\kappa}c_0$ , and  $L_{L-1,\ell} = \sqrt{\kappa}c_{L-1}$ , similarly for the pump  $L_{0,g} = \sqrt{\Gamma}c_0^\dagger$  and  $L_{L-1,g} = \sqrt{\Gamma}c_{L-1}^\dagger$ .
- [52] We note that, on the other hand, the fact that  $J_+ + J_-$  is complex does not induce any non-reciprocal or unidirectional dynamics since the imaginary part of the Hamiltonian is proportional to the kinetic energy and not the current.
- [53] J. Dalibard, Y. Castin, and K. Mølmer, *Phys. Rev. Lett.* **68**, 580 (1992).
- [54] M. B. Plenio and P. L. Knight, *Rev. Mod. Phys.* **70**, 101 (1998).
- [55] A. J. Daley, *Adv. Phys.* **63**, 77 (2014).
- [56] R. D. Soares and M. Schirò, *SciPost Phys.* **17**, 128 (2024).

- [57] M. Bukov, M. Kolodrubetz, and A. Polkovnikov, *Phys. Rev. Lett.* **116**, 125301 (2016).
- [58] K. Seetharam, P. Titum, M. Kolodrubetz, and G. Refael, *Phys. Rev. B* **97**, 014311 (2018).
- [59] F. Peronaci, M. Schiró, and O. Parcollet, *Phys. Rev. Lett.* **120**, 197601 (2018).
- [60] T. Haga, M. Nakagawa, R. Hamazaki, and M. Ueda, *Phys. Rev. Lett.* **127**, 070402 (2021).
- [61] A. Kamenev, *Field theory of non-equilibrium systems* (Cambridge Univesity Press, Cambridge, 2023).
- [62] F. Thompson and A. Kamenev, *Ann. Phys. (N. Y.)* **455**, 169385 (2023).
- [63] G. T. Landi, M. J. Kewming, M. T. Mitchison, and P. P. Potts, *PRX Quantum* **5**, 020201 (2024).
- [64] L. Amico, R. Fazio, A. Osterloh, and V. Vedral, *Rev. Mod. Phys.* **80**, 517 (2008).
- [65] B. Xing, X. Turkeshi, M. Schiró, R. Fazio, and D. Poletti, *Phys. Rev. B* **109**, L060302 (2024).
- [66] I. Poboiko, P. Pöpperl, I. V. Gornyi, and A. D. Mirlin, *Phys. Rev. B* **111**, 024204 (2025).

## END MATTER

### INTERACTING CASE: DYNAMICS WITH OPEN BOUNDARY CONDITIONS

We present additional results on the interacting problem, in particular concerning the dynamics of particle density with OBC. In the main text, we have explored the dynamics along the line  $\phi = \theta$  with  $\Gamma = \kappa$ , where the effective single particle hopping is reciprocal, while the gain induces a non-reciprocal distribution function leading to charge accumulation. Here instead we fix  $\theta = -\phi$ , corresponding to non-reciprocal hoppings  $J_+ \neq J_-$  in the non-interacting model (see Fig. 2(e) in the main text) and plot in Fig. 4 the dynamics of particle density for different values of the interaction  $\Delta$ , starting from a charge density wave initial state. We see that the CDW pattern quickly melts after few coherent revivals at short-times. Furthermore, the directional dynamics observed in the non-interacting case, with a bump in the density profile traveling from the left edge of the system, remains well defined for moderate value of the interaction  $\Delta < J$ . The effect of  $\Delta$  is to increase the damping of this mode which already for  $\Delta = 0.5J$  does not travel far enough to reach the boundary and melts down in the bulk of the chain. For  $\Delta > J$ , on the other hand, the directionality of the dynamics is barely visible, and the initial CDW state rapidly approaches a uniform steady state.

### ENTANGLEMENT ENTROPY OF QUANTUM TRAJECTORIES

Here we discuss the entanglement structure of our model of non-reciprocal, driven-dissipative fermions. The density matrix  $\rho(t)$  solution of the Lindblad master equa-

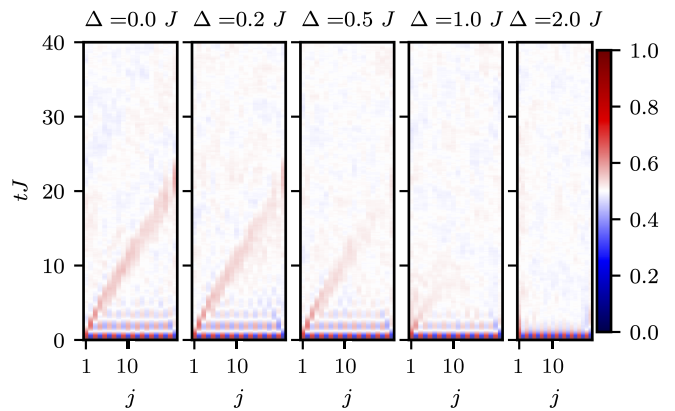


Figure 4. Dynamics of particle density with OBC for different values of the interaction  $\Delta$  and for  $\phi = -\theta = \pi/2$ , corresponding to non-reciprocal hoppings  $J_+ \neq J_-$  in the single particle non-Hermitian Hamiltonian controlling the unconditional evolution. Other parameters:  $L = 20$  and  $\Gamma = \kappa = 0.1J$

tion defined in the main text describes, in general, a mixed state. In order to characterize entanglement and quantum correlations, we therefore use an unraveling of the system density matrix  $\rho(t)$  into many-body quantum trajectories [29, 47, 53–55]. These describe the non-unitary, but purity-preserving, evolution of the system conditioned to a series of measurement outcomes associated to the set of jump operators  $L_{j\mu}$ . Given a quantum trajectory  $|\psi(\xi_t, t)\rangle$  evolving under the quantum jumps dynamics, we introduce the conditional density matrix  $\rho(\xi_t, t) = |\psi(\xi_t, t)\rangle\langle\psi(\xi_t, t)|$ . Upon averaging this quantity over the measurement noise  $\xi_t$ , one recovers the mixed density matrix solution of the Lindblad master equation, i.e.  $\rho(t) = \int |\psi(\xi_t, t)\rangle\langle\psi(\xi_t, t)|$ .

As long as one is interested in standard average quantities  $\langle O \rangle = \text{Tr}(\rho(t)O)$ , the conditional and average (also called unconditional) state contain the same information. However, this is not the case for quantities that involve non-linear functions of the state, for instance, probing higher moments of the conditional density matrix  $\rho(\xi_t, t)$ . A relevant example is provided by the von Neumann entanglement entropy, defined as [64]

$$S_A(t, \xi_t) = -\text{tr}_A [\rho_\xi^A(t) \ln \rho_\xi^A(t)] \quad (11)$$

where we have introduced a bipartition  $A \cup B$  of the system and defined the reduced density matrix  $\rho^A(\xi_t, t) = \text{tr}_B |\psi(\xi_t, t)\rangle\langle\psi(\xi_t, t)|$ . In the following, we are interested in the average entanglement entropy, given by  $\bar{S}_A(t) = \int \mathcal{D}\xi P(\xi) S_A(\xi_t, t)$  where the average is taken over the Poisson measurement noise  $\xi_t$ . Clearly, the average entanglement entropy does not generally coincide with the entanglement entropy of the average state. The former is known to undergo a non-trivial evolution under continuous monitoring, leading to measurement-induced phase transitions. In the present context, we focus on the effect of interaction and non-reciprocity on the dy-

namics of the entanglement entropy. In Fig. 5(a) we plot the time-evolution of the average entanglement entropy for a bipartition of size  $L/2$ , different system sizes at fixed angles  $\theta = \phi = \pi/2$  and for both  $\Delta = 0$  (non-interacting fermions) and  $\Delta = 2J$ . Interestingly, we note that while in the non-interacting case the entanglement entropy has a very weak dependence on system size and saturates to a constant area-law value, for  $\Delta \neq 0$  the entanglement dynamics depends clearly on the size of the subsystem. At long-times, the entanglement saturates to a steady-state value that depends linearly on  $L$  (see inset), i.e. the scaling is compatible with a volume-law. For interacting monitored quantum many-body systems, volume-law scaling of entanglement entropy is expected, at least for weak monitoring [65, 66]. However, this is rather surprising in the present context of non-reciprocal fermions, given the fact that from the point of view of the steady state the charge is localized at the boundary as in the skin-effect [24]. Next, we explore the dependence of the entanglement entropy dynamics from the non-reciprocity, by tuning the angles  $\theta, \phi$  for  $\Delta = 0$  (Fig. 5b) and  $\Delta = 2J$  (Fig. 5c). By comparing the two panels, we first note that in the fully reciprocal case, corresponding to  $\theta = \phi = 0$ , the entanglement dynamics depends only weakly on the interaction  $\Delta$ . Non-reciprocity, on the other hand, suppresses the entanglement growth in the non-interacting case, an effect which is significantly less pronounced in the interacting non-reciprocal case, whose entanglement content appears to be more robust.

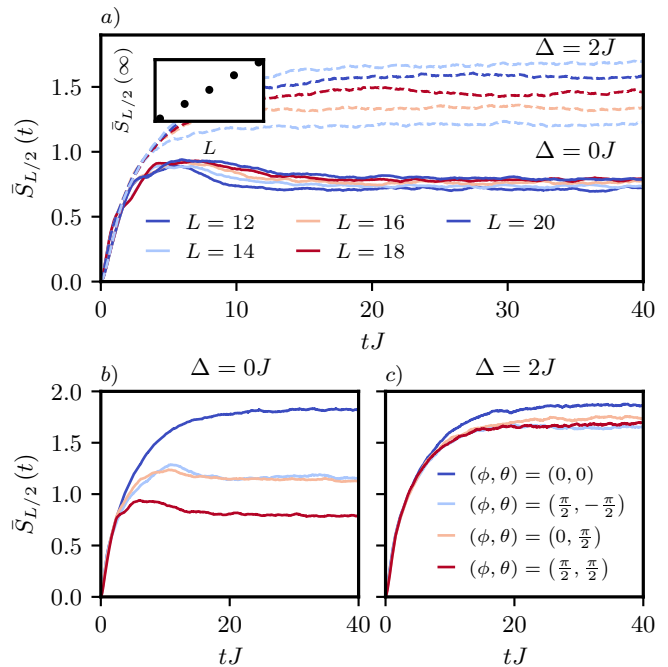


Figure 5. *a*) - Time evolution of the average entanglement entropy for different system sizes and interaction strength with  $\phi = \theta = \pi/2$ . *b*) and *c*) - Time evolution of the entanglement entropy for different values of the angles for  $L = 20$ . Panel *b*) corresponds to the non-interacting case, while in *c*)  $\Delta = 2.0J$ . The label is shared between panel *b*) and *c*). Other parameters:  $\Gamma = \kappa = 0.1J$ .

# Supplemental Material to ‘Steady-state non-reciprocal transport in an interacting fermionic chain’

## Symmetries of the Lindblad Master Equation

We briefly discuss the symmetries associated with the Lindblad master equation and the jump operators defined in the main text. In addition to a standard weak U(1) symmetry, where the fermionic operators can be rotated by an arbitrary global phase  $c_j \rightarrow e^{i\alpha} c_j$  without changing the master equation, the system also features a local gauge symmetry associated with the phases  $\phi, \theta$ . In particular under PBC and local transformation

$$c_j \rightarrow e^{ir_j\theta} c_j, \quad c_j^\dagger \rightarrow e^{-ir_j\theta} c_j^\dagger \quad (\text{S1})$$

where  $r_j$  is the position of the site  $j$ , one can eliminate the phase  $\theta$  from the gain term, whose jump operators transform as

$$L_{j,g} \rightarrow \sqrt{\Gamma} e^{-ir_j\theta} (c_j^\dagger + c_{j+1}^\dagger), \quad (\text{S2})$$

giving rise to a gain-dissipator which is independent of  $\theta$ . At the same time, the loss term acquires a  $\theta$  dependence,

$$L_{j,\ell} \rightarrow \sqrt{\kappa} e^{ir_j\theta} (c_j + e^{i(\phi+\theta)} c_{j+1}), \quad (\text{S3})$$

and similarly, the hopping term acquires a Peierls-like phase

$$-\frac{J}{2} (c_j^\dagger c_{j+1} + \text{h.c.}) \rightarrow -\frac{J}{2} (e^{i\theta} c_j^\dagger c_{j+1} + \text{h.c.}). \quad (\text{S4})$$

In other words, our model with non-reciprocal gain and losses is equivalent to a model with momentum-dependent (but reciprocal) gain, non-reciprocal losses with a phase  $\theta + \phi$  and non-reciprocal hopping due to a Peierls phase  $e^{i\theta}$ . However, we note that, while the phase  $\theta$  can be eliminated from the Lindbladian, it still affects physical observables which need to be transformed as well. Finally, we stress that our model in the absence of interaction  $\Delta = 0$  has particle-hole symmetry for  $\Gamma = \kappa$  and  $\phi = \theta$  since in this case the master equation is invariant under  $c_j \leftrightarrow c_j^\dagger$ . A finite  $\Delta$  gives rise to a shift in the Hamiltonian  $\delta H = -2\Delta \sum_i n_i$ .

## Non-Interacting Case: Equations of Motion and Continuity Equation

In this section, we discuss in more detail the non-interacting limit ( $\Delta = 0$ ). We provide additional details that support the results discussed in the main text for both open-boundary and periodic boundary conditions. First, we write the equation of motion for the point correlation function,

$$\begin{aligned} i\partial_t \langle c_n^\dagger c_m \rangle &= -\frac{1}{2} [J + i\kappa e^{i\phi} + i\Gamma e^{-i\theta}] \langle c_n^\dagger c_{m+1} \rangle - \frac{1}{2} [J + i\kappa e^{-i\phi} + i\Gamma e^{i\theta}] \langle c_n^\dagger c_{m-1} \rangle + \\ &+ \frac{1}{2} [J - i\kappa e^{-i\phi} - i\Gamma e^{i\theta}] \langle c_{n+1}^\dagger c_m \rangle + \frac{1}{2} [J - i\kappa e^{i\phi} - i\Gamma e^{-i\theta}] \langle c_{n-1}^\dagger c_m \rangle + \\ &- 2i\kappa \langle c_n^\dagger c_m \rangle + 2i\Gamma (\delta_{n,m} - \langle c_n^\dagger c_m \rangle) + \\ &+ i\frac{\Gamma}{2} (e^{-i\theta} [\delta_{n,m+1} + \delta_{n-1,m}] + e^{i\theta} [\delta_{n,m-1} + \delta_{n+1,m}]). \end{aligned} \quad (\text{S5})$$

As already discussed, both gain and loss dissipation couple to the hopping elements of the unitary evolution, leading to the appearance of two distinct effective hopping rates:  $J_\pm = J + i\kappa e^{\pm i\phi} + i\Gamma e^{\mp i\theta}$ . It is interesting to see how these effective couplings affect the dynamics of the particle density at a site  $n$ ,

$$\partial_t \langle c_n^\dagger c_n \rangle + v_+ \langle \mathcal{I}_n \rangle - v_- \langle \mathcal{I}_{n-1} \rangle + \frac{\langle h_n \rangle + \langle h_{n-1} \rangle}{2J} [\kappa \cos(\phi) + \Gamma \cos(\theta)] = \langle \mathcal{T}_n \rangle, \quad (\text{S6})$$

where  $v_\pm = 1 \pm [\Gamma/J \sin(\theta) - \kappa/J \sin(\phi)]$ ,  $\langle \mathcal{T}_n \rangle = 2\Gamma - 2(\Gamma + \kappa) \langle c_n^\dagger c_n \rangle$  which is the global rate of particle injection/losses from the bath,  $\langle \mathcal{I}_n \rangle$  the expectation value of the local particle current operator at a site  $n$  and  $\langle h_n \rangle$  the expectation value of the local kinetic energy density at a site  $n$ , namely,

$$\langle \mathcal{I}_n \rangle = \frac{iJ}{2} (\langle c_{n+1}^\dagger c_n \rangle - \langle c_n^\dagger c_{n+1} \rangle), \quad \langle h_n \rangle = \langle c_{n+1}^\dagger c_n \rangle + \langle c_n^\dagger c_{n+1} \rangle. \quad (\text{S7})$$

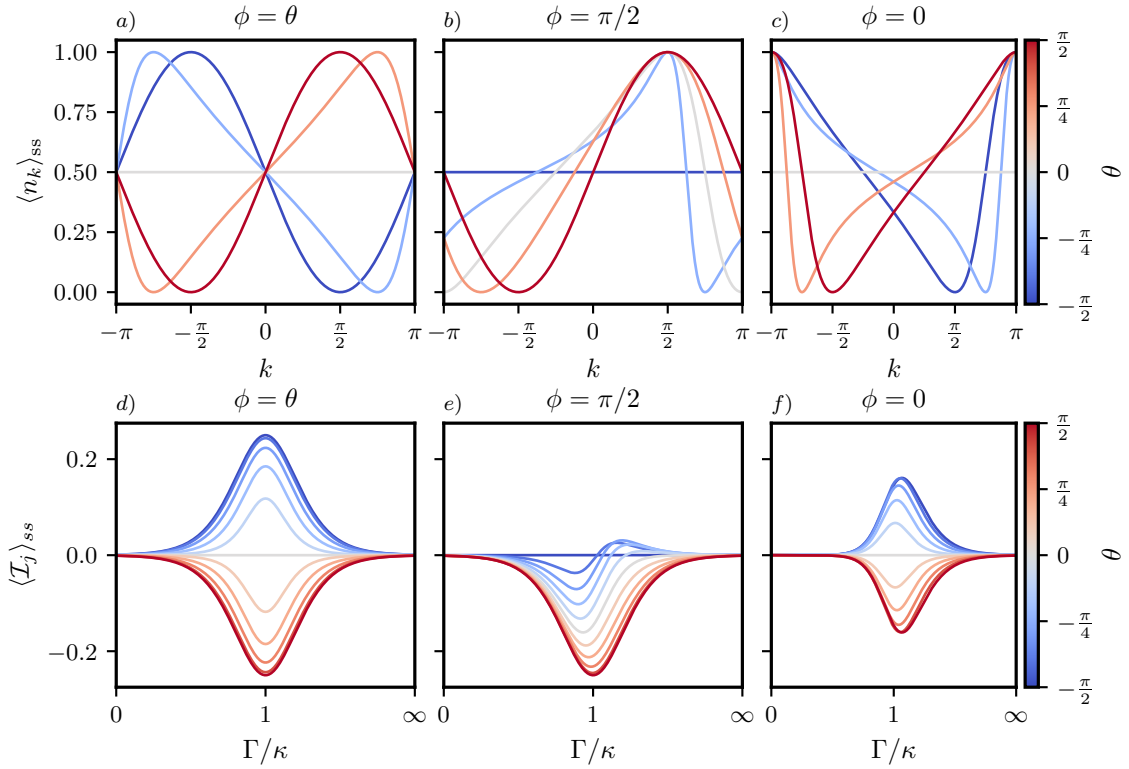


Figure S1. Upper row - Steady-state distribution for different values of the angle  $\theta$  with  $\phi$  fixed with  $\Gamma = \kappa$ . Lower row - Steady-state particle current as a function of the ratio  $\Gamma/\kappa$  for different values of the angle  $\theta$  with  $\phi$  fixed. The  $\Gamma/\kappa$  axis is in log-scale.

Eq. (S6) would describe a local continuity equation associated with global conservation of the total particle number if the system were governed solely by Hamiltonian dynamics. However, the right-hand side of the equation reveals that particles can be injected into or removed from the system due to coupling with the bath. In particular, the imaginary components of the effective hoppings  $J_{\pm}$ , renormalize and induce direction-dependent effective velocities. This is similar to what was observed in certain regimes for the no-click dynamics of the Hatano-Nelson model [56]. In addition, their real part introduces a non-trivial contribution that depends on the local kinetic energy.

As we show next, an imbalance in  $v_{\pm}$  serves as a reliable indicator of directionality in the propagation of the local particle density. This is further evident from the local particle current in the PBC case, where, despite the absence of directional propagation - since the system ultimately reaches homogeneity - directionality can still be inferred from the presence of a net particle current.

### Results for Periodic Boundary Conditions

Here we provide further analytical results for the PBC case in the absence of interactions. In this case, the equation of motion for the correlation matrix Eq. (S5), when written in momentum space  $C_{kq} = \langle c_k^{\dagger} c_q \rangle$ , simplify to

$$\partial_t C_{kq} = - \left[ i(\varepsilon_k - \varepsilon_q) + \frac{\lambda_k + \lambda_q}{2} \right] C_{kq} + \delta_{k,q} \Gamma_k, \quad (\text{S8})$$

with  $\lambda_k = \Gamma_k + \kappa_k$  as defined in the main text, and  $\varepsilon_k = -J \cos(k)$ . The solution corresponds, for the off-diagonal matrix elements, to an exponential decay in time,

$$C_{kq}(t) = C_{kq}(0) e^{-i(\varepsilon_k - \varepsilon_q)t} e^{-(\lambda_k + \lambda_q)t/2}, \quad (\text{S9})$$

while, for the diagonal elements of the correlation matrix (that is the distribution function  $n_k(t) = C_{kk}(t)$ ), we obtain Eq. (6) of the main text. First, we discuss the steady-state solution of these equations of motion. In the steady-state,

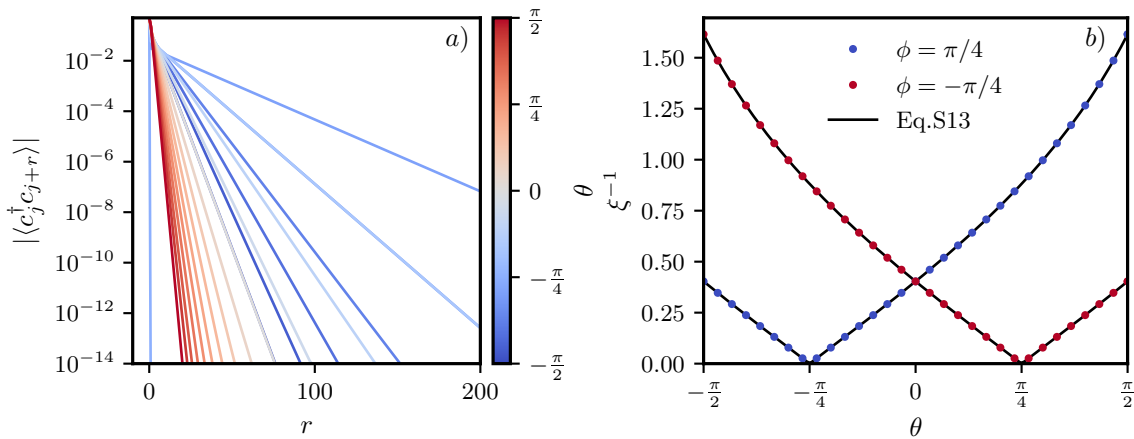


Figure S2. a) - Absolute value of the two-point correlation function as a function of distance  $r$  for  $\phi = \pi/4$ . The correlation length is minimal and equal to zero for  $\theta = -\phi$ . b) - Inverse correlation length as a function as function of  $\theta$  for two distinct values of  $\phi$ . Other parameters:  $\Gamma = \kappa = 0.1J$

the correlation matrix is diagonal in momentum; as such, the steady-state particle density and current are spatially uniform and given by

$$\langle n_j \rangle_{\text{ss}} = \int_{-\pi}^{+\pi} \frac{dk}{2\pi} \langle n_k \rangle_{\text{ss}}, \quad \langle \mathcal{I}_j \rangle_{\text{ss}} = -J \int_{-\pi}^{+\pi} \frac{dk}{2\pi} \sin(k) \langle n_k \rangle_{\text{ss}}, \quad (\text{S10})$$

where the steady-state distribution is given in Eq. (8) of the main text, that we rewrite here as a function of the angles  $\theta, \phi$  and the ratio between the gain and loss rate  $\kappa/\Gamma$

$$\langle n_k \rangle_{\text{ss}} = \frac{(1 + \cos(k - \theta))}{(1 + \cos(k - \theta)) + \frac{\kappa}{\Gamma} (1 + \cos(\phi + k))}. \quad (\text{S11})$$

In Fig. S1, we plot the distribution function  $\langle n_k \rangle_{\text{ss}}$  for different values of the angles (top row) and the corresponding particle current as a function of  $\Gamma/\kappa$  and the two angles (bottom row). As mentioned in the main text, the steady state does not support a particle current when the momentum distribution  $\langle n_k \rangle_{\text{ss}}$  is flat in  $k$ , which occurs along the line  $\phi = -\theta$ . In this case, as seen from Eq. (S11), the two dissipative processes interfere destructively and cancel out, leaving a distribution function  $\langle n_k \rangle_{\text{ss}} = \Gamma/\Gamma + \kappa$ , which is identical to the case of local onsite gain ( $L_{j,g} = \sqrt{\Gamma}c_j^\dagger$ ) and losses ( $L_{j,\ell} = \sqrt{\kappa}c_j$ ). In contrast, the particle current is maximized when  $\langle n_k \rangle_{\text{ss}} = (1 + \sin(k))/2$ , which occurs for  $\theta = \phi = \pm\pi/2$  and  $\Gamma = \kappa$ , as clearly seen in the lower row of Fig. S1 and in Fig. 2.(c) of the main text. In this case, the modes with the highest group velocity are the most populated, resulting in a maximal current. As the angles are tuned away from this line, the distribution function loses the (anti)symmetry with respect to inversion, thus reducing the current. Moreover, as shown in the figure, the particle current vanishes in both limits  $\Gamma/\kappa \rightarrow 0$  and  $\Gamma/\kappa \rightarrow \infty$ , corresponding to a fully empty and fully filled chain, respectively, and reaches its maximum at  $\Gamma = \kappa$ . The sign of the current is controlled by both angles but also by the gain/loss ratio. This is seen in Fig. S1.(e), where for some angles  $\theta$  and a fixed  $\phi = \pi/2$ , the current can be reversed by increasing the gain/loss ratio. When  $\theta = \phi$ , we can derive an analytical expression for the particle current, also assuming that  $\Gamma = \kappa$ ,

$$\langle \mathcal{I}_j \rangle_{\text{ss}} = J \frac{\sin(\theta)}{2 \cos^2(\theta)} (|\sin(\theta)| - 1), \quad (\text{S12})$$

in this case, the direction of the particle current is given by the sign of the  $\sin(\theta)$ .

It is also interesting to explore other correlation functions. We note that the steady state is never critical: the steady-state two-point correlation function always decays exponentially,  $\langle c_j^\dagger c_{j+r} \rangle \propto e^{-r/\xi}$ , with a correlation length  $\xi$  that remains finite throughout the phase diagram for all system parameters. This correlation length depends sensitively on the angles and exhibits a non-monotonic dependence as one angle is varied relative to the other, as shown in Fig. S2.(a). This can be analytically determined through the poles of the distribution  $\langle n_k \rangle_{\text{ss}}$ , which indicate

that

$$\xi^{-1} = \frac{1}{2} \log \left( \frac{\Gamma + \kappa + 2\sqrt{\Gamma\kappa} \left| \sin \left( \frac{\theta + \phi}{2} \right) \right|}{\Gamma + \kappa - 2\sqrt{\Gamma\kappa} \left| \sin \left( \frac{\theta + \phi}{2} \right) \right|} \right). \quad (\text{S13})$$

We note that this expression is not valid for  $\theta = -\phi$ . As one approaches the line  $\theta = -\phi$  the dissipative gap  $\delta$  decreases toward zero, leading to an increasing correlation length. However, right at the critical line,  $\delta = 0$ , also the gain vanishes in the same way, giving rise to a completely flat momentum distribution in  $k$  space, i.e.  $\langle c_j^\dagger c_{j+r} \rangle = \delta_{r,0}$ .

For what concerns the transient dynamics, we first consider an initially empty lattice such that the dynamics of particle density and current does not depend on initial off diagonal correlations in momentum space. As such, the particle density and coherent current at a site  $j$  can be formally obtained by using,

$$\langle n_j(t) \rangle = \int_{-\pi}^{+\pi} \frac{dk}{2\pi} \langle n_k(t) \rangle, \quad \langle \mathcal{I}_j(t) \rangle = -J \int_{-\pi}^{+\pi} \frac{dk}{2\pi} \sin(k) \langle n_k(t) \rangle, \quad (\text{S14})$$

where the time dependent distribution function is given in Eq. (6) of the main text. We start by considering the line  $\phi = -\theta$ , for which we have  $\lambda_k = 2(\Gamma + \kappa)[1 + \cos(k + \phi)]$ . In this case we can rewrite the particle density as

$$\begin{aligned} \langle n_j(t) \rangle &= \frac{\Gamma}{\Gamma + \kappa} \left( 1 - e^{-2(\Gamma + \kappa)t} \int_{-\pi}^{+\pi} \frac{dk}{2\pi} e^{-2(\Gamma + \kappa) \cos(k + \phi)t} \right) \\ &= \frac{\Gamma}{\Gamma + \kappa} \left( 1 - e^{-2(\Gamma + \kappa)t} \sum_{n=-\infty}^{+\infty} \int_{-\pi}^{+\pi} \frac{dk}{2\pi} \left( -ie^{i(k + \phi)} \right)^n J_n(2i(\Gamma + \kappa)t) \right) \\ &= \frac{\Gamma}{\Gamma + \kappa} \left( 1 - e^{-2(\Gamma + \kappa)t} I_0(2(\Gamma + \kappa)t) \right), \end{aligned} \quad (\text{S15})$$

where  $I_0(\cdot)$  is the zero order Bessel Function of the second kind. Similarly, for the current, we get

$$\langle \mathcal{I}_j(t) \rangle = -\frac{\Gamma}{\Gamma + \kappa} I_1(2(\Gamma + \kappa)t) e^{-2(\Gamma + \kappa)t} \sin(\phi), \quad (\text{S16})$$

with  $I_1(\cdot)$  the first order Bessel Function of the second kind. As mentioned in the main text, we see that there is a transient current as long as  $\phi \neq n\pi$ , even though in the steady-state the current vanishes. We also see that the direction is controlled by the angle  $\phi$ .

In the limit  $t \rightarrow +\infty$ , we can expand the Bessel functions and obtain the asymptotics of particle density and current

$$\begin{aligned} \langle n_j(t \rightarrow \infty) \rangle &= \frac{\Gamma}{\Gamma + \kappa} \left( 1 - \frac{1}{2\sqrt{\pi}\sqrt{\Gamma + \kappa}} \sqrt{\frac{1}{t}} \right) + O(t^{-3/2}), \\ \langle \mathcal{I}_j(t \rightarrow \infty) \rangle &= \frac{\Gamma}{2\sqrt{\pi}(\Gamma + \kappa)^{3/2}} \sin(\phi) \sqrt{\frac{1}{t}} + O(t^{-3/2}). \end{aligned} \quad (\text{S17})$$

In both cases, we obtain a power-law decay towards the steady-state value (which is zero for the current) of the form  $1/t^\alpha$  with an exponent  $\alpha = 1/2$ . This decay is ultimately due to the fact that the spectrum of decay rates  $\lambda_k$  vanishes quadratically around  $k_*$ . On the other hand, away from the line  $\theta = -\phi$ , the spectrum  $\lambda_k$  is gapped,  $\lambda_k = \delta + \alpha(k - k_*)^2$  and the dynamics of both particle density and current acquire an additional exponential decay with a scale controlling the distance from the critical line  $\phi = -\theta$ .

### Dynamics for an initial charge density wave state

In this subsection, we discuss the time evolution of the particle and the current density for an initial state in a charge-density wave (CDW), as done in the main text. When considering periodic boundary conditions, in the thermodynamic limit, the initial state correlation matrix in momentum space can be written as

$$\langle c_k^\dagger c_q \rangle = \frac{1}{2} \delta_{k,q} + \frac{1}{2} \delta_{k+\pi,q}. \quad (\text{S18})$$

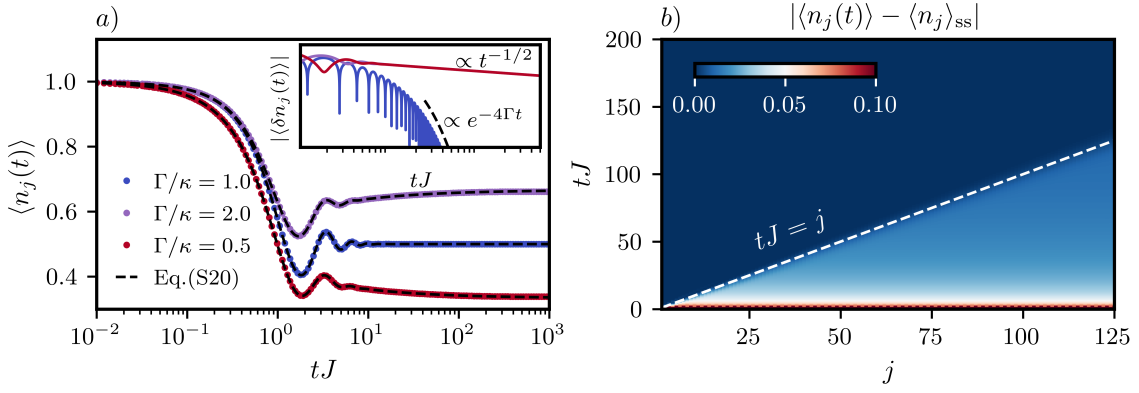


Figure S3. Time evolution of the local particle density from a CDW initial state. *a*) Comparison of the analytical expression and numerical results for various ratios of  $\Gamma/\kappa$  under PBC. The inset illustrates the approach to the steady state via  $\langle \delta n_j(t) \rangle = \langle n_j(t) \rangle - \langle n_j \rangle_{ss}$ . *b*) Time evolution of the local particle density for  $\Gamma = 0.5J$  and  $\kappa = 0.1J$  in a system with OBC. Other simulation parameters:  $\phi = -\theta = \pi/2$ .

As such, the particle density and particle current, for all angles, are given by,

$$\begin{aligned} \langle n_j(t) \rangle &= \langle n_j \rangle_{ss} + \frac{1}{2} \int_{-\pi}^{\pi} \frac{dk}{2\pi} \left[ \left( 1 - \frac{2\Gamma_k}{\Gamma_k + \kappa_k} \right) e^{-\lambda_k t} + (-1)^j e^{-2(\Gamma+\kappa)t - 2i\varepsilon_k t} \right], \\ \langle \mathcal{I}_j(t) \rangle &= \langle \mathcal{I}_j \rangle_{ss} - \frac{J}{2} \int_{-\pi}^{\pi} \frac{dk}{2\pi} \left[ \left( 1 - \frac{2\Gamma_k}{\Gamma_k + \kappa_k} \right) e^{-\lambda_k t} \sin(k) + (-1)^j e^{-2(\Gamma+\kappa)t} \sin(k - 2\varepsilon_k t) \right]. \end{aligned} \quad (\text{S19})$$

These integrals can be analytically solved in the same way as before (Eq. (S15)) by using the Jacobi–Anger expansion. First, we consider the regime where  $\theta = -\phi$ . Along this specific line of angles, the dynamics starting from an initial CDW for the local particle density and particle current are given by

$$\begin{aligned} \langle n_j(t) \rangle &= \frac{\Gamma}{\Gamma + \kappa} + \left[ \frac{1}{2} - \frac{\Gamma}{\Gamma + \kappa} \right] e^{-2(\Gamma+\kappa)t} I_0(2[\Gamma + \kappa]t) + \frac{(-1)^j}{2} e^{-2(\Gamma+\kappa)t} J_0(2Jt), \\ \langle \mathcal{I}_j(t) \rangle &= - \left[ \frac{1}{2} - \frac{\Gamma}{\Gamma + \kappa} \right] I_1(2(\Gamma + \kappa)t) e^{-2(\Gamma+\kappa)t} \sin(\phi) - \frac{(-1)^j}{2} e^{-2(\Gamma+\kappa)t} J_1(2Jt), \end{aligned} \quad (\text{S20})$$

where  $I_\alpha(\cdot)$  and  $J_\alpha(\cdot)$  are the  $\alpha$ -order modified Bessel function of the first kind and the  $\alpha$ -order Bessel function of the first kind, respectively. For all values of  $\Gamma$  and  $\kappa$ , the initial charge density wave order vanishes exponentially fast, as seen by the second term in the equation. However, the way in which the particle density reaches the steady state can be altered by tuning the ratio  $\Gamma/\kappa$ . Specifically, in the long-time limit, both the particle density and current approach the steady state following a power law given by  $t^{-1/2}$ , as long as  $\Gamma \neq \kappa$ ,

$$\begin{aligned} \langle n_j(t \rightarrow \infty) \rangle - \langle n_j \rangle_{ss} &= \frac{\kappa - \Gamma}{4\sqrt{\pi}(\Gamma + \kappa)^{3/2}} \sqrt{\frac{1}{t}} + O(t^{-3/2}), \\ \langle \mathcal{I}_j(t \rightarrow \infty) \rangle - \langle \mathcal{I}_j \rangle_{ss} &= \frac{\Gamma - \kappa}{4\sqrt{\pi}(\Gamma + \kappa)^{3/2}} \sin(\phi) \sqrt{\frac{1}{t}} + O(t^{-3/2}). \end{aligned} \quad (\text{S21})$$

In contrast, when both  $\Gamma = \kappa$ , the relaxation is exponentially fast

$$\begin{aligned} \langle n_j(t \rightarrow \infty) \rangle - \langle n_j \rangle_{ss} &= \frac{(-1)^j}{2} e^{-2(\Gamma+\kappa)t} J_0(2Jt), \\ \langle \mathcal{I}_j(t \rightarrow \infty) \rangle - \langle \mathcal{I}_j \rangle_{ss} &= -\frac{(-1)^j}{2} e^{-2(\Gamma+\kappa)t} J_1(2Jt), \end{aligned} \quad (\text{S22})$$

as we show in the inset of Figure S3(a) for the particle density. For a generic initial state, one observes a power-law decay toward the steady state for all values of the ratio  $\Gamma/\kappa$ . The exponential behavior seen here is a unique consequence of our initial condition, since the diagonal elements of the correlation matrix are the same in the initial

state and in the steady-state  $\langle c_k^\dagger c_k(0) \rangle = \langle c_k^\dagger c_k \rangle_{\text{ss}}$ . As a result, the average total number of particles remains conserved throughout the evolution, and the external bath only leads to the decay of the off-diagonal elements of the correlation matrix,  $\langle c_k^\dagger c_q \rangle$ .

We now discuss the dynamics with OBC. In this case, we see a clear front in the propagation of the particle density, which is consistent with recent results [32]. At short times, we see that both OBC and PBC show qualitatively similar dynamics; however, in the long-time limit, the system under open boundary conditions shows an extra exponential decay, as observed in the panel of Fig. S3.

The model studied in this work belongs to the class of Lindbladians that display the Liouville skin-effect [32, 60], and so, as already stressed in previous works [32], the spectrum and eigenmodes of the Lindblad superoperator under open and periodic conditions are substantially different, leading, as a consequence, to quite distinct dynamics.

### Keldysh Approach

Here we discuss the solution of the non-interacting problem  $\Delta = 0$  with Keldysh techniques and the resulting Green's functions describing dynamical correlations above the steady-state. We start rewriting the Lindblad master equation in the main text as a path integral over fermionic coherent fields defined on the Keldysh contour  $\psi_{ja}, \bar{\psi}_{ja}$ , where  $j$  is the lattice site and  $a = \pm$  labels the contour branch [29, 42, 61, 62]. We have

$$\mathcal{Z} = \int \mathcal{D}\psi \mathcal{D}\bar{\psi} e^{i\mathcal{S}[\psi, \bar{\psi}]}, \quad (\text{S23})$$

where the Keldysh action, in real space, reads

$$\mathcal{S}[\psi, \bar{\psi}] = \int dt \sum_{ja} a \bar{\psi}_{ja} i \partial_t \psi_{ja} - \left( \sum_a a H_a[\psi, \bar{\psi}] + iD[\psi, \bar{\psi}] \right), \quad (\text{S24})$$

with  $H$  the Hamiltonian, written in terms of the coherent fields, and  $D[\cdot]$ , the dissipator which is given by

$$D[\psi, \bar{\psi}] = \sum_{j\mu} \bar{L}_{j\mu-} L_{j\mu+} - \frac{1}{2} (\bar{L}_{j\mu+} L_{j\mu+} + \bar{L}_{j\mu-} L_{j\mu-}), \quad (\text{S25})$$

where  $L_{j\mu a}, \bar{L}_{j\mu a}$  are the jump operators on site  $j$  and  $\mu = \ell, g$  describes loss/gain processes. The action in momentum-frequency space takes the form

$$\mathcal{S}[\psi, \bar{\psi}] = \sum_k \int d\omega \bar{\Psi}_k \begin{pmatrix} \omega - \varepsilon_k + i(\kappa_k - \Gamma_k)/2 & i\Gamma_k \\ -i\kappa_k & -\omega + \varepsilon_k + i(\kappa_k - \Gamma_k)/2 \end{pmatrix} \Psi_k, \quad (\text{S26})$$

where we have defined the field  $\bar{\Psi}_k = (\bar{\psi}_{k+} \ \bar{\psi}_{k-})$ , and the momentum-dependent gain and loss rates are defined in the main text. From this action we can compute the Green's function in the  $\pm$  basis, defined as

$$\hat{G}_k(t, t') = -i \langle \Psi_k(t) \bar{\Psi}_k(t') \rangle = \begin{pmatrix} G_k^{++} & G_k^{+-} \\ G_k^{-+} & G_k^{--} \end{pmatrix}. \quad (\text{S27})$$

The Green functions in frequency/momentum space is given by the inverse of the Gaussian action and reads

$$\hat{G}(k, \omega) = \begin{pmatrix} \omega - \varepsilon_k + i(\kappa_k - \Gamma_k)/2 & i\Gamma_k \\ -i\kappa_k & -\omega + \varepsilon_k + i(\kappa_k - \Gamma_k)/2 \end{pmatrix}^{-1}, \quad (\text{S28})$$

It is convenient to introduce the retarded, advanced and Keldysh components,  $G^{R,A,K}(k, \omega)$  which are directly related to the spectrum and the occupation of the excitations above the steady-state [61]. These are given by

$$G^{R/A}(k, \omega) = \frac{1}{\omega - \varepsilon_k \pm i\lambda_k/2}, \quad G^K(k, \omega) = \frac{i(\Gamma_k - \kappa_k)}{(\omega - \varepsilon_k)^2 + \lambda_k^2/4}, \quad (\text{S29})$$

From the retarded Green function, we can compute the spectral function  $A(k, \omega) = -(1/\pi) \text{Im} G^R(k, \omega)$  of the fermions,

$$A(k, \omega) = \frac{1}{2\pi} \frac{\lambda_k}{(\omega - \varepsilon_k)^2 + \lambda_k^2/4}, \quad (\text{S30})$$

which takes the form of a Lorentzian with a momentum-dependent broadening given by the spectrum of decay rates  $\lambda_k$  defined in the main text. This broadening, which reflects the finite lifetime of excitations due to the coupling with the external baths, is minimal at  $k_*(\theta, \phi)$  and equal to the dissipative gap, while it vanishes along the critical line  $\theta = -\phi$ . Here, the excitations above the steady-state are sharp coherent quasiparticles

$$A(k^*, \omega) = \delta(\omega - \varepsilon_{k^*}). \quad (\text{S31})$$

The dissipative transition in the dynamics discussed in the main text appears therefore as a transition in the spectral function of the fermions. This also translates into a transition in the decay of the local retarded Green's function in the time-domain,  $G^R(x=0, t) = \int dk d\omega e^{-i\omega t} G^R(k, \omega)$  from exponential for  $\theta \neq -\phi$  to power-law  $G^R(x=0, t) \sim 1/\sqrt{t}$ . We note that the decay is slower than the usual  $1/t$  decay of free fermions.

The Keldysh component of the Green function allows us to define an out of equilibrium distribution function  $f(k, \omega)$  from an effective fluctuation-dissipation theorem [61]

$$f(k, \omega) = -\frac{G^K(k, \omega)}{2\pi i A(k, \omega)} = \frac{\kappa_k - \Gamma_k}{\lambda_k}. \quad (\text{S32})$$

and consequently an effective temperature which, in general, depends on both  $k$  and  $\omega$  and it is defined by the relation

$$\frac{\kappa_k - \Gamma_k}{\lambda_k} = \tanh\left(\frac{\omega}{2T_{\text{eff}}}\right). \quad (\text{S33})$$

However, in the regime where both  $\Gamma = \kappa$  and  $\theta = -\phi$ ,  $T_{\text{eff}} \rightarrow +\infty$ .

### Lindbladian in the Rotating Frame and Doublon only Dynamics

Here we briefly discuss the dynamics in the regime  $\Delta \gg J$ . To this extent it is convenient to perform a unitary transformation and move into a rotating frame, i.e., define a new density matrix  $\tilde{\rho} = V\rho V^\dagger$  with  $V$  unitary operator of the form

$$V = \exp(-iKt), \quad (\text{S34})$$

and  $K$  a suitable operator. In this frame the Lindblad equation for the density matrix  $\tilde{\rho}$  reads

$$\partial_t \tilde{\rho} = -i \left[ \tilde{\mathcal{H}}, \tilde{\rho} \right] + \sum_{j\mu} \tilde{L}_{j\mu} \tilde{\rho} \tilde{L}_{j\mu}^\dagger - \frac{1}{2} \left\{ \tilde{L}_{j\mu}^\dagger \tilde{L}_{j\mu}, \tilde{\rho} \right\}, \quad (\text{S35})$$

where we have defined respectively the rotated Hamiltonian  $\tilde{\mathcal{H}}$

$$\tilde{\mathcal{H}} = i(\partial_t V) V^\dagger + V H V^\dagger, \quad (\text{S36})$$

and the rotated jump operators

$$\tilde{L}_{j\mu} = V L_{j\mu} V^\dagger, \quad \tilde{L}_{j\mu}^\dagger = V L_{j\mu}^\dagger V^\dagger. \quad (\text{S37})$$

We choose the unitary as

$$V = \exp(-i\Delta Dt), \quad (\text{S38})$$

where  $D = \sum_i n_i n_{i+1}$  is the total number of next-neighbor doublons. This is picked, so that, the rotated Hamiltonian does not contain anymore the interaction term [58, 59], namely

$$\tilde{\mathcal{H}} = i(\partial_t V) V^\dagger + V \mathcal{H} V^\dagger = V \mathcal{H}_0 V^\dagger \quad (\text{S39})$$

with  $\mathcal{H}_0 = -\frac{J}{2} \sum_{j=0}^{L-2} [c_j^\dagger c_{j+1} + c_{j+1}^\dagger c_j]$ . The price to pay is the rotation of single particle operators in the frame generated by  $V$ . After simple manipulation these take the form

$$V c_j V^\dagger = c_j e^{i\Delta(n_{j-1} + n_{j+1})t}. \quad (\text{S40})$$

We see from this expression that the dressed destruction operator now gains a phase factor that depends on the occupation of neighboring sites. In particular, starting from an occupied site  $i$  we see that if either  $j - 1$  or  $j + 1$  are occupied, that is, in the presence of a doublon, the destruction operator gets a phase that rapidly oscillates at large  $\Delta$  and thus averages out. Similarly for the creation operator we get

$$Vc_j^\dagger V^\dagger = c_j^\dagger e^{-i\Delta(n_{j-1}+n_{j+1})t}. \quad (\text{S41})$$

As a consequence the hopping term entering the renormalized Hamiltonian reads

$$\tilde{\mathcal{H}} = V\mathcal{H}_0V^\dagger = \sum_j e^{-i\Delta t(n_{j-1}-n_{j+2})} c_j^\dagger c_{j+1} + \text{h.c.}, \quad (\text{S42})$$

For what concerns the dissipative processes, we see that the dressed loss term corresponds to

$$\tilde{L}_{j,\ell} = \sqrt{\kappa}(e^{i\Delta(n_{j-1}+n_{j+1})t}c_j + e^{i\phi}e^{i\Delta t(n_j+n_{j+2})t}c_{j+1}), \quad (\text{S43})$$

while the gain reads

$$\tilde{L}_{j,g} = \sqrt{\Gamma}(e^{-i\Delta(n_{j-1}+n_{j+1})t}c_j^\dagger + e^{i\theta}e^{-i\Delta t(n_j+n_{j+2})t}c_{j+1}^\dagger). \quad (\text{S44})$$

In the rotated frame, the dynamics is described by a correlated hopping process with correlated gain and losses. In particular, coherent evolution contains resonant hopping processes between sites  $j, j + 1$  that conserve the doublon number (if  $n_{j-1} = n_{j+2}$ ) and off-resonant ones, for  $n_{j-1} \neq n_{j+2}$ , which rapidly oscillate at frequency  $\Delta$  and average out for  $\Delta \gg J$  leading to doublon-only dynamics. In this regime, both gain and loss processes are also kinetically blocked, as they can only connect states that differ in doublon number and thus dissipate with a rapidly oscillating phase. As a result, for  $\Delta \gg J$ , the dynamics become increasingly coherent, and charge accumulation at the boundary is suppressed, as we observe numerically.

### Methods: Quantum Trajectories and Faber Polynomials

To solve both the dynamics and the steady-state correlation functions of the interacting model, we unravel the Lindblad master equation into quantum trajectories [55]. This approach is numerically more efficient, as it avoids evolving the full density matrix by instead simulating a smaller set of states from which the Lindblad dynamics are recovered through averaging.

In the following, we describe the quantum jump dynamics of the many-body Lindbladian in Eq. (2) by unravelling the master equation using quantum jump trajectories. Specifically, we introduce the pure state  $|\psi(\xi_t, t)\rangle$  which evolves according to the stochastic Schrödinger equation,

$$d|\psi_{\xi_t}(t)\rangle = -idt \left[ \mathcal{H} - \frac{i}{2} \sum_{j,\mu} \left( L_{j,\mu}^\dagger L_{j,\mu} - \langle L_{j,\mu}^\dagger L_{j,\mu} \rangle_t \right) \right] |\psi_{\xi_t}(t)\rangle + \sum_{j,\mu} \left( \frac{L_{j,\mu}}{\sqrt{\langle L_{j,\mu}^\dagger L_{j,\mu} \rangle}} - 1 \right) d\xi_{j,\mu,t} |\psi(\xi_t, t)\rangle, \quad (\text{S45})$$

where  $\langle \circ \rangle_t \equiv \langle \psi(\xi_t, t) | \circ | \psi(\xi_t, t) \rangle$ , and  $\xi_t = \{\xi_{j,\mu,t}\}$  represent a collection of independent Poisson processes  $d\xi_{j,\mu,t} \in \{0, 1\}$  characterized by the mean  $\overline{d\xi_{j,\mu,t}} = dt \langle L_{j,\mu}^\dagger L_{j,\mu} \rangle_t$ . This dynamic arises from a sequence of random quantum jumps, causing sudden changes in the wave function, alongside a deterministic, non-unitary evolution governed by a non-Hermitian Hamiltonian

$$\mathcal{H}_{\text{nh}} = \mathcal{H} - \frac{i}{2} \sum_{j,\mu} L_{j,\mu}^\dagger L_{j,\mu}. \quad (\text{S46})$$

If one considers the average of the pure state density matrix over all quantum jump trajectories, the resulting density matrix takes the form i.e.

$$\rho(t) = \overline{|\psi(\xi_t, t)\rangle \langle \psi(\xi_t, t)|}, \quad (\text{S47})$$

which evolves according to the Lindblad master equation written in Eq. (2). In order to perform the non-Hermitian evolution between consecutive quantum jumps, we make use of the recently developed Faber polynomial method [56].

The dynamics of each quantum trajectory is numerically simulated by combining the high-order Monte Carlo Wave Function algorithm [55, 63] with the Faber polynomial algorithm presented in [56]. In particular, between quantum jumps, the state's non-unitary evolution is expanded using a Faber polynomial series expansion of the time evolution operator

$$e^{-i\mathcal{H}_{\text{nH}}t} |\Psi(t_0)\rangle = \sum_{n=0}^{+\infty} c_n(t) F_n\left(\frac{\mathcal{H}_{\text{nH}}}{\lambda}\right) |\Psi(t_0)\rangle, \quad c_n(t) = e^{-i\lambda\gamma_0 t} \left(\frac{-i}{\sqrt{\gamma_1}}\right)^n J_n(2\sqrt{\gamma_1}\lambda t), \quad (\text{S48})$$

where  $F_n(\cdot)$  is the  $n^{\text{th}}$  Faber Polynomial,  $J_n(\cdot)$  is the  $n^{\text{th}}$  Bessel function of the first kind,  $\lambda$  is a rescaling parameter and  $\gamma_0$  and  $\gamma_1$  are related with the bounds of the spectrum of the non-Hermitian Hamiltonian (for further details check consult [56]). We never explicitly compute the  $F_n(\mathcal{H}_{\text{nH}}/\lambda)$ , but rather do it implicit when acting on the states using the recurrence relation satisfied by the polynomials,

$$\begin{aligned} |\Psi_0\rangle &= |\Psi(t_0)\rangle, \\ |\Psi_1\rangle &= \left(\frac{\mathcal{H}_{\text{nH}}}{\lambda} - \gamma_0\right) |\Psi_0\rangle, \\ |\Psi_2\rangle &= \left(\frac{\mathcal{H}_{\text{nH}}}{\lambda} - \gamma_0\right) |\Psi_1\rangle - 2\gamma_1 |\Psi_0\rangle, \\ |\Psi_{n+1}\rangle &= \left(\frac{\mathcal{H}_{\text{nH}}}{\lambda} - \gamma_0\right) |\Psi_n\rangle - \gamma_1 |\Psi_{n-1}\rangle, \quad n > 2, \end{aligned} \quad (\text{S49})$$

where  $|\Psi_n\rangle = F_n(\mathcal{H}_{\text{nH}}/\lambda) |\Psi(t_0)\rangle$ . As discussed in Ref. [56], the computational demand of comes from acting with the operation of multiplying a state by the Hamiltonian matrix, which has a linear cost with the Hilbert space dimension (as long as the Hamiltonian matrix is sparse on some basis). Moreover, the memory cost also scales linearly as only two vectors,  $|\Psi_{n-1}\rangle$  and  $|\Psi_n\rangle$ , must be saved in memory.